

A thermomechanical constitutive model for an epoxy based shape memory polymer and its parameter identifications

Kai Yu · Amber J.W. McClung ·
Gyaneshwar P. Tandon · Jeffrey W. Baur · H. Jerry Qi

Received: 21 January 2013 / Accepted: 29 June 2013 / Published online: 9 April 2014
© Springer Science+Business Media Dordrecht 2014

Abstract This paper presents a three-dimensional (3D) finite deformation thermomechanical model to study the glass transition and shape memory behaviors of an epoxy based shape memory polymer (SMP) (Veriflex E) and a systematic material parameter identification scheme from a set of experiments. The model was described by viscoelastic elements placed in parallel to represent different active relaxation mechanisms around glass transition temperature in the polymer. A set of standard material tests was proposed and conducted to identify the model parameter values, which consequently enable the model to reproduce the experimentally observed shape memory (SM) behaviors. The parameter identification procedure proposed in this paper can be used as an effective tool to assist the construction and application of such 3D multi-branch model for general SMP materials.

Keywords Shape memory effect · Shape memory polymer · Constitutive model

1 Introduction

Shape memory polymers (SMPs) are polymeric smart materials featured by the ability to recover their permanent shape from one (or sometimes multi-programmed Xie 2010;

K. Yu · H. Jerry Qi (✉)
Department of Mechanical Engineering, University of Colorado, Boulder, CO 80309, USA
e-mail: qih@colorado.edu

A.J.W. McClung · G.P. Tandon · J.W. Baur (✉)
Air Force Research Laboratory, Materials and Manufacturing Directorate, WPAFB, Dayton, OH 45433,
USA
e-mail: Jeffery.Baur@wpafb.af.mil

A.J.W. McClung
National Research Council Research Associate, AFRL, Wright-Patterson AFB, Dayton, OH 45433,
USA

G.P. Tandon
University of Dayton Research Ins., Dayton, OH, USA

Xie et al. 2009; Yu et al. 2012; Li and Xie 2011) temporary shape(s) when a proper stimulus is applied (such as heat—Lendlein and Kelch 2002; Liu et al. 2007; Chung et al. 2008; Gall et al. 2005; Mather et al. 2009; Yu et al. 2011; Castro et al. 2010, 2011; Westbrook et al. 2010a; Wang et al. 2011; Ge et al. 2012, 2013, light—Jiang et al. 2006; Koerner et al. 2004; Lendlein et al. 2005; Scott et al. 2005, 2006, magnetic fields—Mohr et al. 2006; Buckley et al. 2006; Schmidt 2006; He et al. 2011; Kumar et al. 2010; Yu et al. 2013, and moisture—Huang et al. 2005; Jung et al. 2006, etc.). This phenomenon is referred to as the shape memory (SM) effect, and has also been observed in some metallic alloys and ceramics. Compared with the shape memory alloys and ceramics, SMPs possess the advantages of high strain recovery (Wei et al. 1998), low density, low cost, easy shape programming procedure, and easy control of recovery. They are also chemically tunable to achieve biocompatibility and biodegradability. Overall, they have gained extensive research interests recently in various fields such as medical, civil, and aerospace engineering (Yakacki et al. 2007; Lendlein and Kelch 2005; Chen and Lagoudas 2008; Liu et al. 2004; Ding et al. 2007; Alvine et al. 2009).

For thermally activated SMPs, the glass transition is the shape memory mechanism. The inherent complexity of polymer SM effects that involve strong temperature sensitivity and multiple shape changing events makes the traditional build-and-test approach for SMP materials and devices design prohibitively inefficient (Nguyen et al. 2010), and hence requires the development of constitutive models that are not only able to predict the polymer behaviors, but also to allow a viable strategy to measure or identify the material parameters on common lab equipment. The early modeling efforts for the most commonly used thermally induced SMPs were one-dimensional, small strain, rheological models which could capture the characteristic SM behavior but with limited prediction capability (Tobushi et al. 1996, 1998; Bhattacharyya and Tobushi 2000; Morshedian et al. 2005). Recently, the phase evolution modeling approach was proposed and considered to be an effective tool to explain some thermomechanical properties of SMPs (Chen and Lagoudas 2008; Barot et al. 2008; Liu et al. 2006; Qi et al. 2008; Long et al. 2009, 2010c; Ge et al. 2011; Westbrook et al. 2010b). This concept can be applied to a wide variety of SMP materials, such as crystallizable (Barot et al. 2008; Ge et al. 2011; Westbrook et al. 2010b, 2011) or photo-activated (Long et al. 2009, 2010a, 2010b, 2011; Ryu et al. 2012) SMPs, but it fails to physically relate the polymer glass transition behavior to their SM effect. In this regards, thermoviscoelastic modeling approaches (Yu et al. 2012; Castro et al. 2010; Ge et al. 2012; Westbrook et al. 2011; Diani et al. 2006; Nguyen et al. 2008; Srivastava et al. 2010) have emerged for the modeling of SMPs in which the mobility of polymer chains can be correlated with viscosity or relaxation time of a Maxwell element. The viscous strain developed at temperature above T_g is restricted at temperature below T_g (temporary shape fixing) (Yu et al. 2012). Reheating to above T_g will reduce the viscosity, reactive dashpot and allows the structure to relax to its equilibrium configuration, which leads to shape recovery. With the modeling concept of glass transition, more comprehensive three-dimensional thermoviscoelastic models have been developed (Westbrook et al. 2011; Diani et al. 2006; Nguyen et al. 2008; Srivastava et al. 2010). Moreover, to capture the multiple relaxation processes in a real polymer system, multi-branch models (resembling the 1D generalized viscoelastic model or Prony series) should be applied (Engels et al. 2009), especially for some polymers with complex glass transition behaviors.

Veriflex E is a commercially available shape memory polymer with a great potential for aerospace and other engineering applications. Several experimental studies (Castro et al. 2011; McClung et al. 2012, 2013) were conducted and showed rather complicated behaviors, which have not been studied theoretically in the past. For example, Castro et al. (2011)

and McClung et al. (2012, 2013) found that the recovery time depended on the programming temperature, which was not observed in many other SMPs. In this paper, we use a more general multi-branch modeling frame to model the thermomechanical properties of the Veriflex E SMP. The model consists of three groups of branches to respectively describe the polymer equilibrium, rubbery and glassy behaviors. One critical aspect in using multi-branch models is how to identify material parameters for the springs and dashpots. We demonstrate that by using a set of standard material tests conducted by McClung et al. (2012, 2013), including stress relaxation, dynamic mechanical analysis (DMA), thermal expansion (CTE) experiments and isothermal tension tests, the material parameters for the rheological elements can be fully determined. The experimentally parameterized model shows the capability to reproduce the observed SM effect. The simulation and experimental results are also compared and discussed. The accompanied strategy for material parameter identifications illustrated in this paper will serve as a standard procedure to construct constitutive models for different SMP materials in a complex number of temperature and time events with finite number of model parameters.

2 Constitutive model

In this section, we briefly present the constitutive model. More details of this modeling frame can be found in Westbrook et al. (2011).

2.1 Overall model description

Figure 1 shows the 1D rheological representation of the applied multi-branch model. A thermal expansion component is arranged in series with mechanical elements, which consist of an equilibrium branch and several non-equilibrium branches placed in parallel. The equilibrium branch is a hyperelastic spring to represent the equilibrium behavior of SMPs. Each non-equilibrium branch is a nonlinear Maxwell element with an elastic spring and a dashpot placed in series. In the set of nonequilibrium branches, m branches are used to represent the relaxation behavior of the glassy mode, and the remaining n non-equilibrium branches are used to represent the relaxation processes in the rubbery state. It should be noted that, as will be shown later in this paper, the difference between the rubbery branches and the glassy branches is that the glassy branches possess yielding behavior whilst rubbery branches do not. In the i th ($1 \leq i \leq m + n$) non-equilibrium branch, the initial moduli of the springs are denoted as E^i and the relaxation times of the dashpot are τ^i ($1 \leq i \leq m$ represents the glassy branch and $m + 1 \leq i \leq m + n$ represents the rubbery branch).

As demonstrated by Holzapfel (2000), the total deformation gradient of the model \mathbf{F} can be decomposed as:

$$\mathbf{F} = \mathbf{F}_M \mathbf{F}_T, \tag{1}$$

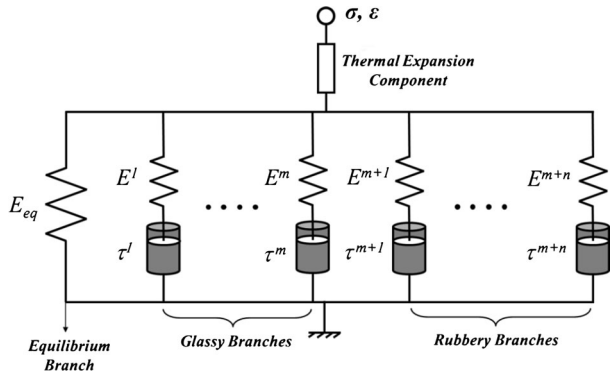
where \mathbf{F}_M is the mechanical deformation gradient and \mathbf{F}_T is the thermal deformation gradient.

The total Cauchy stress of the model $\boldsymbol{\sigma}$ is

$$\boldsymbol{\sigma} = \boldsymbol{\sigma}_{eq} + \sum_{i=1}^{m+n} \boldsymbol{\sigma}^i, \tag{2}$$

where $\boldsymbol{\sigma}_{eq}$ and $\boldsymbol{\sigma}^i$ are the Cauchy stresses in the equilibrium and the i th ($1 \leq i \leq m + n$) non-equilibrium branches, respectively.

Fig. 1 1D rheological representation of the model



2.2 Thermal expansion

The thermal expansion or contraction of the constructed thermal component in the model is assumed to be isotropic,¹ i.e.,

$$\mathbf{F}_T = J_T \mathbf{I}, \tag{3}$$

where \mathbf{I} is the second order unit tensor. J_T is the volume change due to thermal expansion/contraction and is defined as:

$$J_T = \frac{V(T, t)}{V_0} = [1 + 3\alpha_r(T - T_0)](1 + \delta), \tag{4}$$

where $V(T, t)$ is the volume at time t and temperature T . V_0 is the reference volume at the reference temperature T_0 . α_r is the linear coefficient of thermal expansion (CTE) in the rubbery state and δ characterizes the deviation of volume from equilibrium volume (Tool 1946, 1948; Tool and Eichlin 1931) and

$$\delta = \frac{V(T, t)}{V_{eq}(T)} - 1, \quad V_{eq}(T) = [1 + 3\alpha_r(T - T_0)]V_0, \tag{5}$$

where δ is calculated by the well-known KAHR 33-parameter (Kovacs et al. 1979).

2.3 Equilibrium branch

The Cauchy stress tensor in the equilibrium branch uses Arruda–Boyce eight chain model (Arruda and Boyce 1993), i.e.,

$$\boldsymbol{\sigma}_{eq} = \frac{nk_B T}{3J_M} \frac{\sqrt{N}}{\lambda_{chain}} \mathcal{L}^{-1}\left(\frac{\lambda_{chain}}{\sqrt{N}}\right) \overline{\mathbf{B}}' + K(J_M - 1)\mathbf{I}, \tag{6a}$$

$$\overline{\mathbf{B}}' = \overline{\mathbf{B}} - 1/3 \text{tr}(\overline{\mathbf{B}})\mathbf{I}, \quad \overline{\mathbf{B}} = \overline{\mathbf{F}}_M \overline{\mathbf{F}}_M^{-T}, \quad \overline{\mathbf{F}}_M = J_M^{-1/3} \mathbf{F}_M, \tag{6b}$$

¹The anisotropy in polymer thermal expansion could be accounted for by using additional thermal expansion components in the model.

$$\lambda_{\text{chain}} = \sqrt{\text{tr}(\bar{\mathbf{B}})/3}, \quad \mathcal{L}(\beta) = \coth \beta - 1/\beta, \tag{6c}$$

where n is the crosslinking density, k_B is Boltzmann’s constant, T is the temperature, N is the number of Kuhn segments between two crosslink sites (and/or strong physical entanglements). The temperature dependent shear modulus $\mu_r(T)$ of the elastomer in the equilibrium state (which is an indication of entropic elasticity) is given by $nk_B T$. K is the bulk modulus and is typically orders of magnitude larger than μ_r to ensure material incompressibility.

2.4 Non-equilibrium branches

Although in Fig. 1 we distinguished the non-equilibrium branches by glassy branches and rubbery branches, we attempted a unified viscous flow rule for all these branches. The difference between the glassy and rubber branches then comes from their definition of flow resistance, or more specifically, the relaxation time. For the rubbery branches, the relaxation time is a function of temperatures only; for the glassy branches, the relaxation time is a function of temperatures as well as stresses, which give to the yielding behavior. For the i th non-equilibrium branch ($1 \leq i \leq m + n$), the deformation gradient can be further decomposed into an elastic part and a viscous part

$$\mathbf{F}_M = \mathbf{F}_e^i \mathbf{F}_v^i \quad (\text{no summation on } i) \tag{7}$$

where \mathbf{F}_v^i is a relaxed configuration obtained by elastically unloading by \mathbf{F}_e^i . The Cauchy stress can be calculated using \mathbf{F}_e^i ,

$$\boldsymbol{\sigma}^i = \frac{1}{J_e^i} [\mathbf{L}_e^i(T) : \mathbf{E}_e^i], \quad \text{for } 1 \leq i \leq m + n, \tag{8a}$$

$$J_e^i = \det(\mathbf{F}_e^i), \quad \mathbf{E}_e^i = \ln \mathbf{V}_e^i, \quad \mathbf{V}_e^i = \mathbf{F}_e^i \mathbf{R}_e^{iT}, \tag{8b}$$

and $\mathbf{L}_e^i(T)$ is the fourth order isotropic elasticity tensor in the i th non-equilibrium branch ($1 \leq i \leq m + n$), which is taken to be temperature independent, in general, i.e.,

$$\mathbf{L}_e^i(T) = 2G^i \left(\mathbf{I} - \frac{1}{3} \mathbf{I} \otimes \mathbf{I} \right) + K^i \mathbf{I} \otimes \mathbf{I}, \quad \text{for } 1 \leq i \leq m + n, \tag{9}$$

where \mathbf{I} is the fourth order identity tensor, G^i and K^i are shear and bulk moduli for each non-equilibrium branch ($1 \leq i \leq m + n$), respectively.

For the rubbery non-equilibrium branches ($m + 1 \leq i \leq m + n$), it is assumed that all the rubbery branches have the same shear modulus, i.e.,

$$G^i(T) = n_R k_B T \quad \text{for } m + 1 \leq i \leq m + n, \tag{10}$$

where n_R is the crosslinking density (Rubinstein and Colby 2003). Since the bulk modulus is used to enforce a nearly incompressible condition, $K^i(T)$ is chosen to be independent of temperatures and be equal to K in the equilibrium branch (Eqs. (6a)–(6c)).

For the glassy non-equilibrium branches ($1 \leq i \leq m$), the shear modulus is taken to be independent of temperatures, i.e.,

$$G^i(T) = \mu_g \quad \text{for } 1 \leq i \leq m, \tag{11a}$$

and $K^i(T)$ is calculated through $G^i(T)$ using the Poisson ratio $\nu^i = \nu_g$,

$$K^i(T) = \frac{2(1 + \nu_g)}{3(1 - 2\nu_g)} \mu_g \quad \text{for } 1 \leq i \leq m. \tag{11b}$$

The elastic modulus in each non-equilibrium branch is calculated as

$$E^i(T) = \frac{G^i(T)}{2(1 + \nu^i)} \quad \text{for } 1 \leq i \leq m + n. \tag{12}$$

In each non-equilibrium branch ($1 \leq i \leq m + n$), the second Piola–Kirchhoff stress in the intermediate configuration (or elastically unloaded configuration) and the Mandel stress are

$$\mathbf{S}^i = J_e^i (\mathbf{F}_e^i)^{-1} \boldsymbol{\sigma}^i (\mathbf{F}_e^i)^{-T} \quad \text{and} \quad \mathbf{M}^i = \mathbf{C}_e^i \mathbf{S}^i, \tag{13}$$

where $\mathbf{C}_e^i = \mathbf{F}_e^{iT} \mathbf{F}_e^i$ is the right Cauchy–Green deformation tensor. Typically for inelastic materials, the Mandel stress is used to drive the viscous flow via the equivalent shear stress,

$$\dot{\gamma}_v^i = \frac{\overline{M}^i}{G^i(T) \tau_M^i(T, \overline{M}^i)}, \tag{14}$$

where the equivalent shear stress is defined as

$$\overline{M}^i = \left[\frac{1}{2} (\mathbf{M}^i)' (\mathbf{M}^i)' \right]^{1/2}, \tag{15}$$

where $(\mathbf{M}^i)' = \mathbf{M}^i - 1/3 \text{tr}(\mathbf{M}^i) \mathbf{I}$. In Eq. (14), the temperature and stress dependent material stress relaxation time $\tau_M^i(T, \overline{M}^i)$ will be discussed in the next section.

The viscous stretch rate \mathbf{D}_v^i is constitutively prescribed to be

$$\mathbf{D}_v^i = \frac{\dot{\gamma}_v^i}{\sqrt{2M^i}} \mathbf{M}^i, \tag{16}$$

where \mathbf{D}_v^i can be made equal to the viscous spatial velocity gradient $l_v^i = \dot{\mathbf{F}}_v^i (\mathbf{F}_v^i)^{-1}$ by ignoring the spin rate \mathbf{W}_v^i and therefore

$$\dot{\mathbf{F}}_v^i = \mathbf{D}_v^i \mathbf{F}_v^i. \tag{17}$$

2.5 Relaxation time and time-temperature shift factor

In the rubbery branches, the temperature dependent relaxation times are calculated according to the thermorheological simplicity principle (Rubinstein and Colby 2003),

$$\tau^i(T) = \tau_0^i \alpha_T(T) \quad \text{for } m + 1 \leq i \leq m + n, \tag{18}$$

where $\alpha_T(T)$ is the time–temperature superposition (TTSP) shift factor and τ_0^i is the relaxation time at the reference temperature when $\alpha_T(T) = 1$. At temperatures around or above T_g , the WLF equation (Williams et al. 1955) is applied,

$$\log \alpha_T(T) = - \frac{C_1(T - T_M)}{C_2 + (T - T_M)}, \tag{19a}$$

where C_1 and C_2 are material constants and T_M is the WLF reference temperature. When the temperature is below T_s , $\alpha_T(T)$ follows the Arrhenius-type behavior (Marzio and Yang 1997):

$$\ln \alpha_T(T) = -\frac{AF_c}{k_b} \left(\frac{1}{T} - \frac{1}{T_g} \right), \tag{19b}$$

where A and F_c are material constants, k_b is Boltzmann’s constant. Here, T_s is calculated by equating $\alpha_T(T)$ in Eqs. (19a) and (19b).

For the glassy branches ($1 \leq i \leq m$), considering the stress induced yield-type behavior at a temperature below T_g , the relaxation time is taken to be a function of temperatures as well as stresses and can be evaluated by an Eyring type of function (Treloar 1958), i.e.,

$$\tau^i(T, \overline{M}^i) = \tau_0^i \alpha_T(T) \exp\left(-\frac{\Delta G^i}{k_B T} \frac{\overline{M}^i}{s^i}\right), \quad \text{for } 1 \leq i \leq m, \tag{20}$$

where, ΔG^i is the activation energy, s^i is the athermal shear strength representing the resistance to the viscoplastic shear deformation in the material, \mathbf{M}^i is Mandel stress, and \overline{M}^i is the equivalent shear stress.

In order to adequately account for the experimentally observed softening effects, the evolution rule for s is defined as

$$\dot{s}^i = h_0^i (1 - s^i/s_s^i) \dot{\gamma}_v^i \tag{21}$$

with $s^i = s_0^i$ when $\dot{\gamma}_v^i = 0$, and s_0^i is the initial value of the athermal shear strength, s_s^i is the saturation value, h_0^i is a prefactor, $\dot{\gamma}_v^i$ is the viscous flow in glassy branches and is defined as $\dot{\gamma}_v^i = \overline{M}^i (G^i(T) \tau^i(T, \overline{M}^i))^{-1}$ ($1 \leq i \leq m$). For the case when $s_0^i > s_s^i$, Eq. (21) represents an evolution rule that characterizes the experimentally observed softening behavior of the material.

3 Material parameter identification and results

3.1 Summary of material parameters and experiments to identify these parameters

All the model parameters mentioned above were identified by using four standard material tests:

1. Stress relaxation tests for identifying parameters associated with TTSP principle.
2. Thermal expansion (CTE) tests for identifying parameters associated with CTE.
3. Dynamic mechanical analysis (DMA) for identifying the initial moduli and the relaxation times at the reference temperature in the non-equilibrium branches.
4. Isothermal tension tests for identifying parameters related yielding and softening in glassy branches and Kuhn segment number in the equilibrium branch.

The final model parameter set, as well as the associated experimental identification methods, are listed in Table 1. The detailed strategy for the parameter identifications are described in the next section.

Table 1 Parameters of the applied constitutive model and the associated identification experiments

Model parameters	Parameter value	Experimental identification method
Parameters in TTSP		
T_g (°C)	95	<i>Stress relaxation tests</i>
T_M (°C)	85	
AF_c/k_b	-24500	
C_1	10.44	
C_2	15.6	
Parameters in thermal expansion		
α_T (1/°C)	3.498×10^{-4}	<i>CTE experiments</i>
T_v (°C)	95	
θ (1/°C)	0.4	
x	0.7	
τ_p (s)	6.5×10^{-3}	
Initial moduli and relaxation times in glassy branches		
$E^1 \sim E^{12}$ (MPa)	99.9	<i>DMA test</i>
$\tau_0^1 \sim \tau_0^{12}$ (s)	128.4	
	1.0×10^{-7}	
	1.5×10^{-2}	
	5.4×10^{-1}	
Initial moduli and relaxation times in rubbery branches		
$E^{13} \sim E^{18}$ (MPa)	5.6	<i>Stress relaxation tests</i>
$\tau_0^{13} \sim \tau_0^{18}$ (s)	2×10^4	
Initial moduli in equilibrium branch		
E_{eq}	0.65	

Table 1 (Continued)

Model parameters	Parameter value	Experimental identification method
Softening parameters in glassy branches		
$\Delta G^1 \sim \Delta G^{12}$ (J)	7.0×10^{-18} 6.6×10^{-19}	9.6×10^{-19} 2.5×10^{-22}
$s_0^1 \sim s_0^{12}$ (Pa)	7.0×10^8 1.0×10^8	3.5×10^8 7.0×10^6
$s_s^1 \sim s_s^{12}$ (Pa)	7.0×10^6 2.0×10^6	4.0×10^6 9.4×10^3
$h_0^1 \sim h_0^{12}$ (Pa)	1.5×10^8 6.0×10^7	6.0×10^7 6.9×10^6
Kuhn segments number in equilibrium branch		
N	6.9	

3.2 Parameters identification process

3.2.1 Stress relaxation tests for parameters in TTSP

The parameters in the TTSP principle were determined by using the stress relaxation tests on the Veriflex E epoxy SMP material. The rectangular sample (20 mm × 3.6 mm × 1 mm) was first subjected to a set of relaxation tests at 34 different temperatures but only curves at 13 temperatures (10, 65, 75, 80, 85, 87.5, 90, 92.5, 95, 100, 105, 110, and 140 °C, respectively) are shown in Fig. 2(a). In each relaxation test, the SMP sample was preloaded by 1×10^{-3} N force to maintain the straightness. After reaching the testing temperature, 30 min were allowed for the thermal equilibrium. For the experimental temperature below 95 °C, the sample was stretched by 0.1 %. Otherwise it was stretched by 2 % on the DMA machine. Then the deformation was maintained during the following 30 minutes. The decay of stress was recorded and the stress relaxation modulus was calculated. Figure 2(a) shows the results of relaxation tests at 13 temperatures on a double logarithmic plot, and the stress relaxation modulus is shown to be strongly dependent on the testing temperature.

The collected data was then shifted into a master curve (Rubinstein and Colby 2003) to represent the polymer stress relaxation behavior over an extended time regime. Previous DMA tests on the Veriflex E SMP material showed that the temperature corresponding to its $\tan \delta$ peak is around 100 °C (McClung et al. 2012). For a typical polymer, the T_g should be about 5–15 °C below $\tan \delta$ peak temperature and T_M (reference temperature in Eq. (19a)) is ~ 10 °C below T_g . Therefore, in the applied multi-branch model, T_g is set to be 95 °C and T_M is 85 °C. Selecting T_M as the reference temperature, each curve in Fig. 2(a) was shifted horizontally to superimpose with the next. This produced the master curve shown in Fig. 2(b), which spans three decades of modulus (from ~ 3000 to ~ 1.7 MPa) and represents the actual relaxation behavior of the epoxy SMPs within a long time scale (~ 1900 years) at 85 °C.

Figure 2(c) shows the shifting factors α_T as a function of temperature. As described in Eqs. (19a) and (19b), the shifting factors follow the WLF and Arrhenius equations when the temperature is respectively above and below T_s . By fitting the experimental data with the theoretical predictions, the parameters in these two equations are determined as: $C_1 = 10.44$, $C_2 = 15.6$, and $AF_c k_B^{-1} = -24500$. The T_s is calculated to be 83.7 °C.

3.2.2 CTE for thermal expansion

The CTE measurement was conducted by using the same tensile setup within the DMA machine. The temperature in the DMA chamber was set to 140 °C for 30 minutes to reach thermal equilibrium. To measure the change in the specimen's length during thermal expansion or contraction, a constant and relatively small tensile force of 1×10^{-3} N was applied and maintained by the top grip during the entire experiment. The temperature was decreased from 140 to 0 °C at a rate of 1 °C/min. After reaching 0 °C, the temperature was then increased to 140 °C at the same rate. This thermal cycle was repeated three times until the experimental curves tended to be stable and only the data from the last cooling step was reported. Figure 3 shows the experimental results of the CTE measurement for the temperature range from 0 to 140 °C. As shown in the figure, the linear regressions at temperatures above and below T_g were taken to be the respective rubbery and glassy linear CTE values. Here the rubbery linear CTE value was determined to be $\alpha_r = 2.893 \times 10^{-4}/^\circ\text{C}$. The structural relaxation parameters were found by fitting the CTE measurement curve through a simulation where a small force as applied to the top surface of the specimen and the temperature

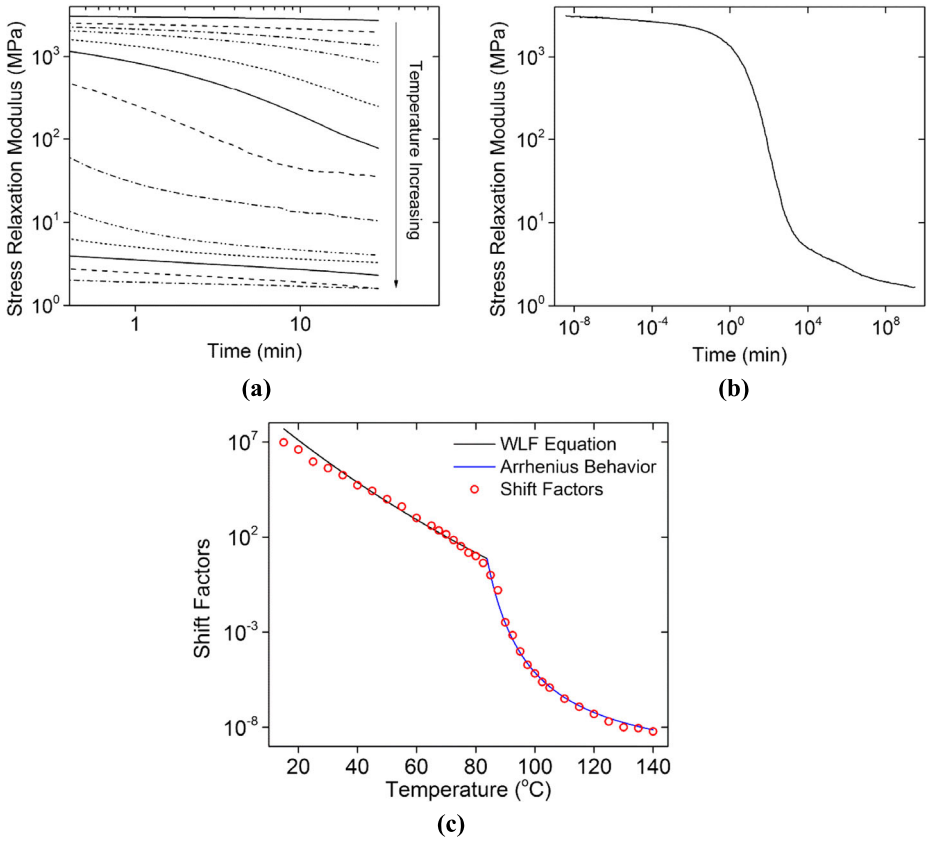
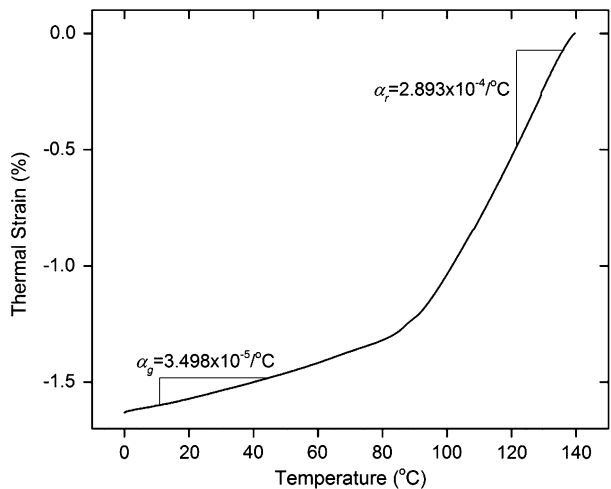


Fig. 2 Stress relaxation tests to determine the material parameters in TTSP: (a) stress relaxation tests at 13 different temperatures (10, 65, 75, 80, 85, 87.5, 90, 92.5, 95, 100, 105, 110, and 140 $^{\circ}\text{C}$, respectively); (b) the stress relaxation master curve at 85 $^{\circ}\text{C}$; (c) shifting factors at different temperatures: above 85 $^{\circ}\text{C}$, shifting factors follow the WLF equation; below 85 $^{\circ}\text{C}$, shifting factors follow the Arrhenius-type behavior

Fig. 3 Experimental results from the thermal expansion experiments (CTE)



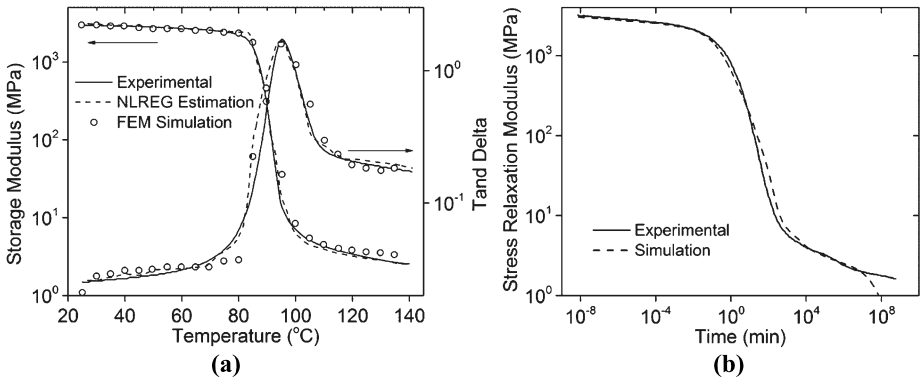


Fig. 4 (a) Comparisons between the experimental results, NLREG estimations and the FEM simulations of the storage modulus and $\tan \delta$ curves. (b) Comparison between the experimental stress relaxation master curve and predictions based on the multi-branch model

was decreased. The detailed parameters identification strategy could be found in Westbrook et al. (2011). The remaining parameters were obtained to be $\theta = 0.43/^\circ\text{C}$, $x = 0.4$, and $\tau_V = 6.5 \times 10^{-3}$ s.

3.2.3 DMA for initial moduli and relaxation times in individual branches

DMA test (TA Instruments, Model Q800) was performed to characterize the glass transition behavior of the Veriflex E epoxy SMP material. The rectangular sample (20 mm \times 3.6 mm \times 1 mm) was first heated to 140 $^\circ\text{C}$ on the DMA machine and stabilized for 20 minutes to reach thermal equilibrium, and then a preload of 1 KPa and an initial strain with a magnitude of 0.1 % was applied. During the experiment, the strain was oscillated at a frequency of 1 Hz with a peak-to-peak amplitude of 0.1 % while the temperature was decreased from 140 to 25 $^\circ\text{C}$ at a rate of 1 $^\circ\text{C}/\text{min}$. The temperature in the chamber was held at 25 $^\circ\text{C}$ for 30 minutes and then increased to 140 $^\circ\text{C}$ again at the same rate. This procedure was repeated multiple times and the data from the last cooling step is reported in Fig. 4(a) (solid line). The temperature corresponding to the peak of $\tan \delta$ curve is shown to be 98 $^\circ\text{C}$. Note that this value is slightly lower than the value reported previously where the heating rate is set as 2 $^\circ\text{C}/\text{min}$ (McClung et al. 2013).

By using nonlinear regression (NLREG) method (Diani et al. 2012; Sherrod 2000), the initial modulus and relaxation time (at 20 $^\circ\text{C}$) in each branch were estimated by fitting the model prediction with the experimental results. For the 1D multi-branch linear model, the temperature dependent storage modulus $E_s(T)$, loss modulus $E_l(T)$ and $\tan \delta(T)$ are respectively expressed as:

$$E_s(T) = E_{eq} + \sum_{i=1}^{m+n} \frac{E^i(T)w^2(\tau^i(T))^2}{1 + w^2(\tau^i(T))^2}, \tag{22a}$$

$$E_l(T) = \sum_{i=1}^{m+n} \frac{E^i(T)w\tau^i(T)}{1 + w^2(\tau^i(T))^2}, \tag{22b}$$

$$\tan \delta(T) = \frac{E_l(T)}{E_s(T)}, \tag{22c}$$

where w is the testing frequency, $\tau^i(T)$ is the relaxation time in each non-equilibrium branch, and $E^i(T)$ is the elastic modulus in each branch. As shown in Eqs. (10)–(12), $E^i(T)$ is temperature independent in the glassy branches and temperature dependent in the rubbery branches where they are defined as linear functions of temperature and the initial modulus E^i at the reference temperature (20 °C). For the convenience of operation, during the NLREG analysis, we assume that the relaxation times in the rubbery branch increase in a tenfold sequential. Non-equilibrium branches are gradually added into the model to improve the prediction, and the branch number is finally determined when the NLREG estimations (shown as dash lines in Fig. 4(a)) could capture the experimental storage and $\tan \delta$ curves within the entire testing temperature range (25–140 °C).

Subsequently, the estimated material parameters were imported into the 3D finite deformation constitutive model described in Sect. 2, which was implemented into a user material subroutine (UMAT) in the finite element software package ABAQUS (Simulia, Providence, RI). Some of the detailed calculation method for the stress and Jacobian tensor can be found in the previous studies of Weber and Anand (1990), Anand and Kothari (1996). Using the implemented UMAT, the DMA tests were simulated by applying a sinusoidal displacement loading on the top surface of an 8-node linear hexahedron thermally coupled brick element (C3D8T) in the ABAQUS element library, while the bottom surface was fixed in the tension direction. After extracting the strain and stress information of the element from the result file, delta value could be determined by measuring the phase lag of the stress curve to the strain curve, and the storage modulus was then calculated accordingly. In Fig. 4(a), results from finite element method (FEM) simulations for the DMA tests are compared to the experimental results. Overall, at different temperatures (from 25 to 135 °C with a 5 °C temperature interval), the material parameters identified from 1D NLREG fit enables the 3D model to capture the experimental storage modulus and $\tan \delta$ curves. In addition, as shown in Fig. 4(b), the relaxation spectrum of the multi-branch model is also able to reproduce the experimental master curve of stress relaxation described in Fig. 2(b) with satisfied accuracy.

3.2.4 Isothermal uniaxial experiments for softening parameters in glassy branches and the Kuhn segment number in the equilibrium branch

To identify the yielding parameters in the glassy branches at different temperatures (25, 60, 90, 100, 110, and 130 °C), experimental data from McClung et al. (2013) was used. Details about experimental setup and procedure can be found in McClung. Figure 5 shows the stress–strain behavior of the Veriflex E epoxy SMP under various temperatures (plotted as solid lines). The experimental results show that the SMP mechanical response highly depends on the strain rate. Besides, it displays a typical hyperelastic behavior in the rubbery region above T_g and typical glassy behavior below T_g . For temperatures below T_g with increasing strain, a yield point is exhibited followed by a post-yield softening behavior.

The stress–strain curves at temperatures below the glassy transition temperature were used to determine the softening parameters in the glassy branches of the model. Before this, the unsoften stress relaxation times in each glassy branch at these three temperatures (25, 60, and 90 °C) were calculated identified by using NLREG and are listed in Table 2. Here, we assume that if the relaxation time is below 0.5 s, the corresponding glassy branch contributes insignificantly to the stress–strain behavior. Therefore, the parameters in that branch cannot be fit. For example, as is shown, at the temperature of 90 °C, only the 11th and 12th glassy branches have relaxation times larger than 0.5 s. Therefore, only the associated softening parameters in these two branches could be determined by fitting the experimental stress–strain curves in Fig. 5(c). For the temperature of 60 °C, branches from 6th to 12th contribute to the

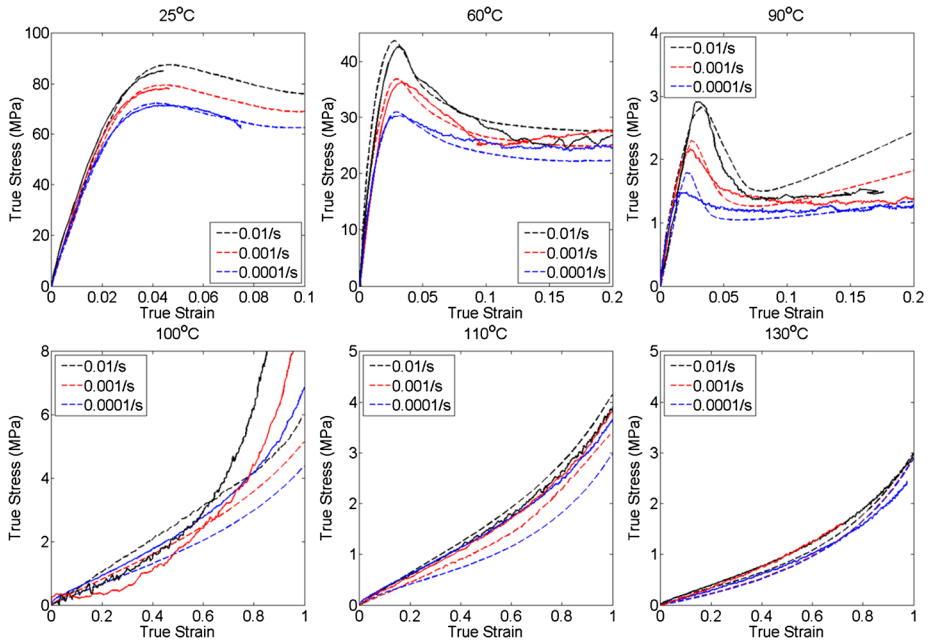


Fig. 5 Stress–strain behavior of Veriflex E epoxy SMP at different temperatures (25, 60, 90, 100, 110, and 130 °C). Note that finite simulations are denoted as *dash lines* and the experimental data is copied from McClung et al. (2013)

Table 2 Relaxation times (s) in each glassy branch at 25, 60, and 90 °C, respectively

Temperature (°C)		90	60	25
Glassy branches	1st	2.92×10^{-10}	1.09×10^{-4}	6.19×10^{-1}
	2nd	2.41×10^{-9}	9.00×10^{-4}	5.09×10^0
	3rd	1.71×10^{-8}	6.38×10^{-3}	3.61×10^1
	4th	1.64×10^{-7}	6.14×10^{-2}	3.47×10^2
	5th	9.84×10^{-7}	3.67×10^{-1}	2.08×10^3
	6th	5.41×10^{-6}	2.02×10^0	1.14×10^5
	7th	4.33×10^{-5}	1.62×10^1	9.17×10^5
	8th	1.58×10^{-3}	5.92×10^2	3.35×10^6
	9th	2.92×10^{-2}	1.09×10^3	6.19×10^7
	10th	2.46×10^{-1}	9.21×10^3	5.21×10^8
	11th	1.74×10^0	6.51×10^5	3.69×10^9
	12th	1.07×10^1	4.02×10^6	2.28×10^{10}

stress–strain curves shown in Fig. 5(b). While keeping the softening parameters unchanged in the 11th and 12th glassy branches, the rest ones (in branches from 6th to 10th) are determined. Similarly, parameters in the 1st to 5th glassy branches are determined by using the experimental curves in Fig. 5(a).

In addition to the softening parameters, the Kuhn segment number of the equilibrium branch N is also identified by using the stress–strain curves in the rubbery region (100, 110,

and 130 °C). For polymeric materials that in the rubbery state, as the stretch ratio approaches a limiting value λ_c^{lim} , the macromolecules are so extended that can no longer accommodate large deformation by rotation (Qi et al. 2003). The stress increases dramatically and strain stiffening occurs. From non-Gaussian chain statistics, this limiting stretch ratio λ_c^{lim} is connected to the number of Kuhn segments in the equilibrium branch by $\lambda_c^{\text{lim}} = \sqrt{N}$. From Figs. 5(e) and 5(f), it is observed that this limiting true strain is around 0.9, and hence the Kuhn segment number of the equilibrium branch is determined to be $N = 6.9$.

Subsequently, the theoretical simulations are compared with the experimental data by introducing an error parameter e in describing their differences:

$$e = \frac{|\sigma_{\text{sim}} - \sigma_{\text{exp}}|}{\sigma_{\text{exp}}} \times 100 \%, \quad (23)$$

where σ_{sim} and σ_{exp} are the stress respectively in the simulations and experiments.

This error is visualized in Fig. 6 as a function of true strain at different temperatures. Overall, the applied 3D multi-branch model is shown to be able to capture the stress–strain behavior of Veriflex E within the entire testing intervals. Relatively high errors are observed when the loading rate is high and the temperature is close to the glass transition temperature. For example, at the temperature of 90 °C and with a loading rate of 0.01/s, the FEM simulation predicts the polymer yield and post-yield behavior well at a low strain level (below 0.1), but deviates from the experimental data subsequently in a manner that the predicted post-yield hardening behavior occurs ahead of the experimental, as shown in Fig. 5(c). In addition, under the loading rate of 0.01/s and 0.001/s, noticeable prediction errors are also found in the 100 °C testing case. One possible reason for this large discrepancy near the glass transition temperature is due to the fact that the material property is very sensitive to the temperature near its glass transition. For example, the modulus can change from 12.7 to 8.3 MPa (a decrease of 34.6 %) when the temperature changes from 95 to 96 °C. Such sensitivity adds a great uncertainty in experimental measurements.

3.3 Model predictions of shape memory behaviors

By far, the material parameters of the 3D multi-branch model are fully determined. In this section, the 3D constitutive model is used to predict the SM behaviors and compare with the experimental observations by McClung et al. (2013). The details on experimental setup and procedure can be found in McClung et al. (2013).

During the experiments, the temperature, strain and stress of the SMP sample were recorded and respectively plotted in solid lines as a function of time in Figs. 7(a) and 7(b). 3D FEA simulations were also performed to describe the SM cycle, predict the free recovery behavior and compare with the experimental results. By using the identified material parameters, the 3D multi-branch model is able to fit the experimental curves well in both the rate of recovery and the time to begin recovery after heating begins, excluding the final shape recovery strain slightly lower than the experimental.

To further demonstrate the effectiveness of the model with the identified material parameters, 3D FEA simulations were conducted to predict the stress–strain and free shape recovery behaviors of Veriflex E SMP under different programming conditions. In the first parametric study, the initial loading rate is set to be 0.5, 5, and 50 mm/min, respectively. Other programming conditions were the same as the baseline case mentioned above. As shown in Fig. 8, the simulation results match with the experimental data well in describing the rate dependent stress–strain behavior as well as the following stress relaxation process.

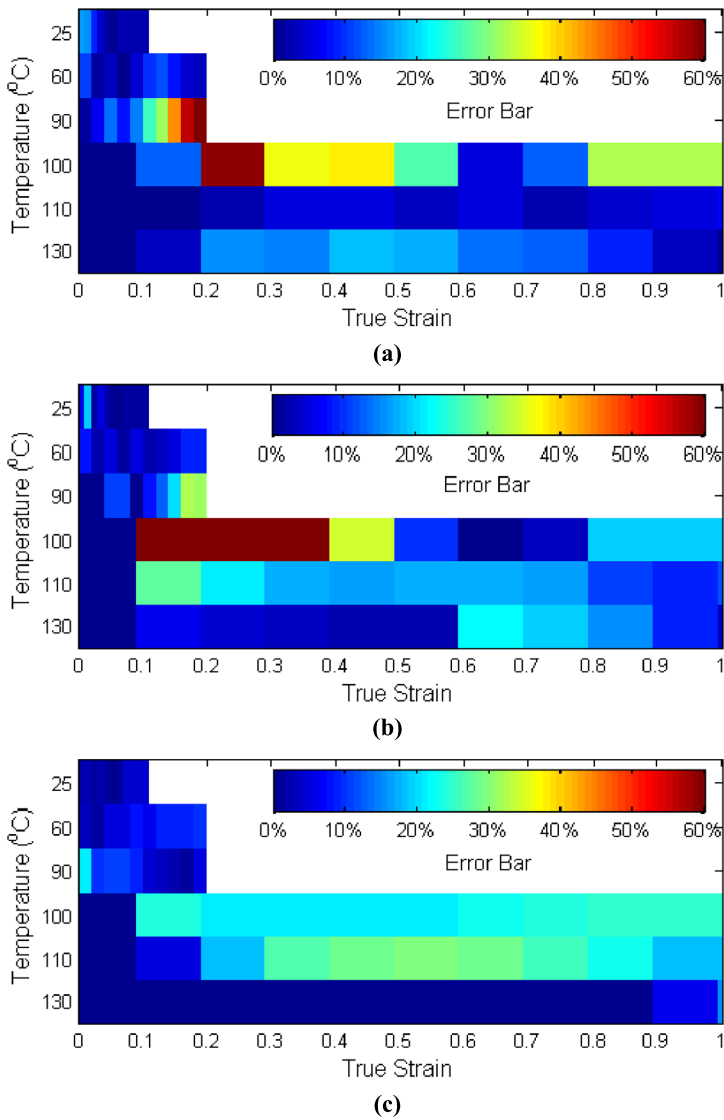


Fig. 6 The prediction error plots as a function of true strain under different testing temperatures. The loading rates are respectively (a) 0.01/s, (b) 0.001/s, and (c) 0.0001/s

In order to qualify the shape fix ability after unloading and the free shape recovery ability for a typical SMP material, the shape fix ratio R_f and shape recovery ratio R_r are respectively defined as:

$$R_f = \frac{\varepsilon_u}{\varepsilon_p} \times 100 \%, \quad (24a)$$

$$R_r = \frac{\varepsilon_p - \varepsilon_f}{\varepsilon_p} \times 100 \%, \quad (24b)$$

Fig. 7 The simulated SM cycle including programming and free recovery steps: **(a)** temperature and stress history, **(b)** strain evolution

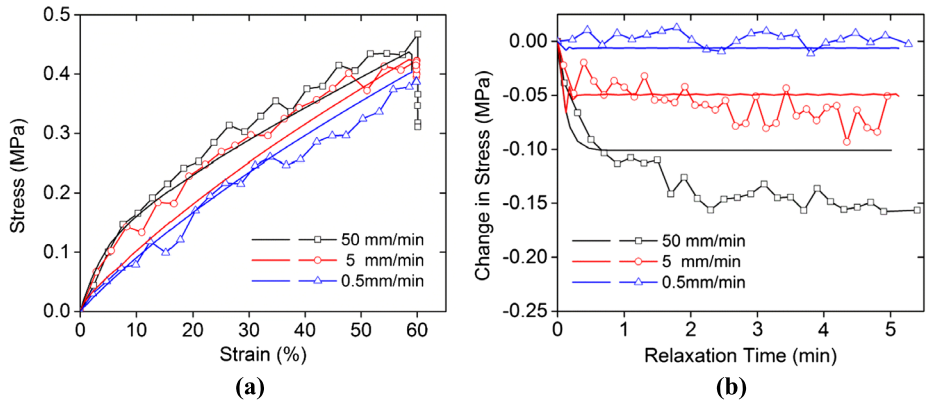
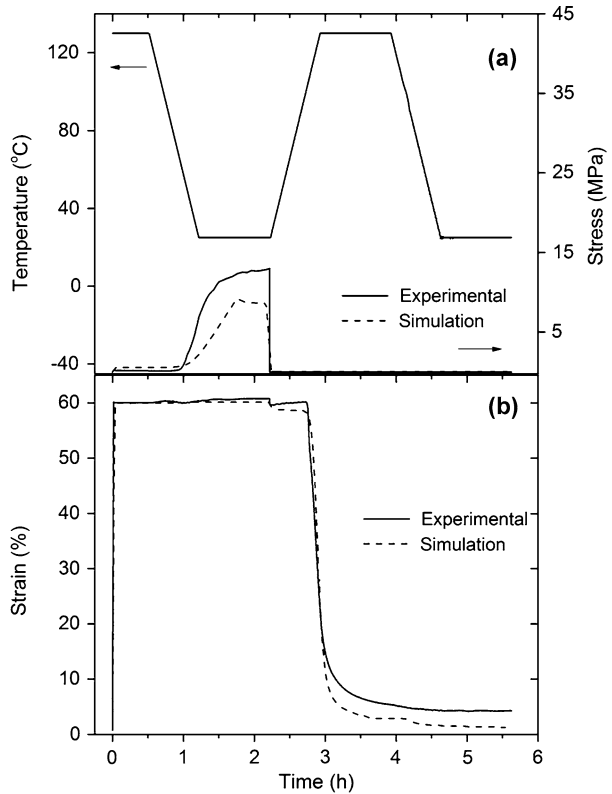
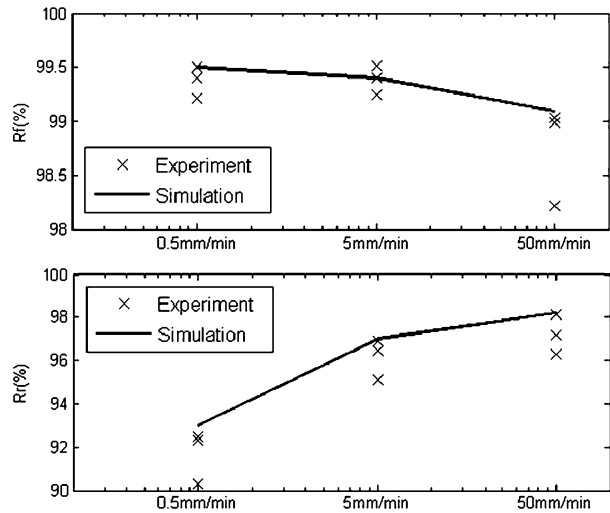


Fig. 8 Tension to 60 % strain at deformation rates of 0.5, 5, and 50 mm/min followed by 5 min stress relaxation periods: **(a)** stress–strain curves and **(b)** change in stress versus relaxation time during relaxation period. Note that the simulation is denoted as *solid lines*

where ϵ_p is the prescribed strain during the programming stretch, ϵ_u is the strain after unloading, and ϵ_f is the final strain at the end of the SM cycle.

During the experiments, three SMP samples are tested for each programming loading rate. The measured shape fix ratio R_f and shape recovery ratio R_r are respectively marked

Fig. 9 Shape fix ratio and shape recovery ratio for programming deformation rates of 0.5, 5, and 50 mm/min (5 min hold time)



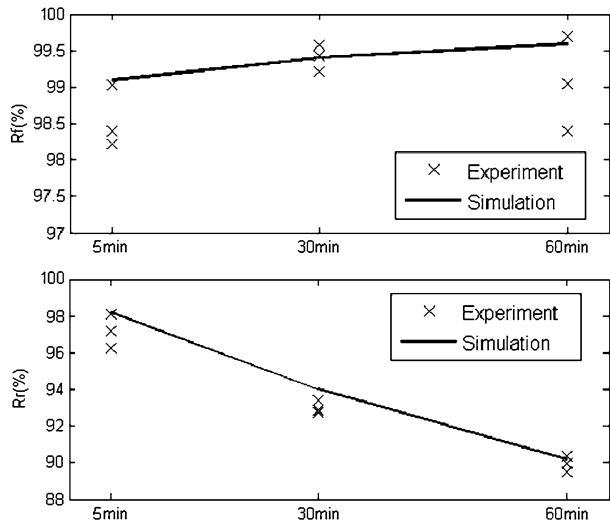
in Fig. 9. Basically, as the increasing of loading rate, the R_f is observed to be decreasing while R_r is increasing. The 3D FEM simulation results (denoted as solid lines in the figure) also accurately reveal this tendency. From the physical point of view, a lower programming loading rate will allow more time for the polymer macromolecules to adjust themselves for the new deformed configurations, and subsequently decrease the system internal energy frozen during cooling (represented as elastic energy in the springs of non-equilibrium branches). Due to the lower energy density state under the action of external load at the low temperature (25 °C), the system will easily reach a new equilibrium state after unloading, which leads to a lower elastic energy loss of the multi-branch model and a higher shape fix ratio. However, when reheating the SMP material, the stored internal energy would provide driving force for the free shape recovery. In this manner, a lower programming loading rate reduces the final shape recovery ratio. This underlying mechanism could also be reflected in the multi-branch model and will be explored in detail in the near future.

In the second parametric study, the holding time at the programming temperature is set to be 5, 30, and 60 min, respectively, while the rest programming conditions are the same as the baseline case. The experimental data, as well as the associated 3D FEM simulations are plotted in Fig. 10. In addition to the agreement between the experimental and simulation results, it is also found the hold time at the programming temperature plays an opposite effect to R_f and R_r in comparison with the programming loading rate. In other words, the polymer SM effect could be affected and controlled equally by decreasing the loading rate or increasing the hold time at the programming temperature.

4 Conclusion

In this paper, a multi-branched model was applied to study the glass transition and shape memory (SM) effect of an amorphous epoxy SMP. The model consists of three groups of parallel branches to respectively characterize the polymer equilibrium, glassy and rubbery non-equilibrium behaviors. According to this modeling frame, three dimensional finite deformation constitutive relations were developed and several sets of material parameters were introduced, which enabled the model to capture sophisticated

Fig. 10 Shape fix ratio and shape recovery ratio for hold times of 5, 30, and 60 min (50 mm/min deformation rate). Note that the simulation is denoted as *solid lines* and the experimental data is denoted as markers



polymer behaviors, as well as to reveal the underlying mechanism. Since each material parameter contributes physical significance to the multi-branch model, they were successively identified by using four standard material tests: stress relaxation tests, dynamic mechanical analysis (DMA), thermal expansion (CTE) experiments and isothermal tension tests. To further demonstrate the effectiveness of the determined material parameters, finite element simulations were conducted based on the multi-branch constitutive model. Comparisons between the simulation results and experimental data showed that the model could capture the experimentally observed polymer SM effect under different programming conditions, which subsequently confirmed the viability of the demonstrated experimental strategy for the material parameters identification.

Acknowledgements H.J.Q. acknowledges the support through AFRL summer faculty fellowship program (contract FA8650-07-D-5800).

References

- Alvine, K.J., et al.: Capillary instability in nanoimprinted polymer films. *Soft Matter* **5**, 2913–2918 (2009)
- Anand, L., Kothari, M.: A computational procedure for rate-independent crystal plasticity. *J. Mech. Phys. Solids* **44**(4), 525–558 (1996)
- Arruda, E.M., Boyce, M.C.: A 3-dimensional constitutive model for the large stretch behavior of rubber elastic-materials. *J. Mech. Phys. Solids* **41**(2), 389–412 (1993)
- Barot, G., Rao, I.J., Rajagopal, K.R.: A thermodynamic framework for the modeling of crystallizable shape memory polymers. *Int. J. Eng. Sci.* **46**(4), 325–351 (2008)
- Bhattacharyya, A., Tobushi, H.: Analysis of the isothermal mechanical response of a shape memory polymer rheological model. *Polym. Eng. Sci.* **40**(12), 2498–2510 (2000)
- Buckley, P.R., et al.: Inductively heated shape memory polymer for the magnetic actuation of medical devices. *IEEE Trans. Biomed. Eng.* **53**(10), 2075–2083 (2006)
- Castro, F., et al.: Effects of thermal rates on the thermomechanical behaviors of amorphous shape memory polymers. *Mech. Time-Depend. Mater.* **14**(3), 219–241 (2010)
- Castro, F., et al.: Time and temperature dependent recovery of epoxy-based shape memory polymers. *J. Eng. Mater. Technol.-Trans. ASME* **133**, 021025 (2011)

- Chen, Y.C., Lagoudas, D.C.: A constitutive theory for shape memory polymers. Part I—large deformations. *J. Mech. Phys. Solids* **56**(5), 1752–1765 (2008)
- Chung, T., Rorno-Urbe, A., Mather, P.T.: Two-way reversible shape memory in a semicrystalline network. *Macromolecules* **41**(1), 184–192 (2008)
- Marzio, E.A., Yang, A.J.M.: Configurational entropy approach to the kinetics of glasses. *J. Res. Natl. Inst. Stand. Technol.* **102**(2), 135–157 (1997)
- Diani, J., Liu, Y.P., Gall, K.: Finite strain 3D thermoviscoelastic constitutive model for shape memory polymers. *Polym. Eng. Sci.* **46**(4), 486–492 (2006)
- Diani, J., et al.: Predicting thermal shape memory of crosslinked polymer networks from linear viscoelasticity. *Int. J. Solids Struct.* **49**(5), 793–799 (2012)
- Ding, Y., et al.: Relaxation behavior of polymer structures fabricated by nanoimprint lithography. *ASC Nano* **1**(2), 84–92 (2007)
- Engels, T.A.P., et al.: Predicting the long-term mechanical performance of polycarbonate from thermal history during injection molding. *Macromol. Mater. Eng.* **294**(12), 829–838 (2009)
- Gall, K., et al.: Thermomechanics of the shape memory effect in polymers for biomedical applications. *J. Biomed. Mater. Res., Part A* **73A**(3), 339–348 (2005)
- Ge, Q., et al.: Thermomechanical behavior of shape memory elastomeric composites. *J. Mech. Phys. Solids* **60**(1), 67–83 (2011)
- Ge, Q., et al.: Prediction of temperature-dependent free recovery behaviors of amorphous shape memory polymers. *Soft Matter* **8**(43), 11098–11105 (2012)
- Ge, Q., et al.: Mechanisms of triple-shape polymeric composites featuring dual thermal transitions. *Soft Matter* **9**, 2212–2223 (2013)
- He, Z.W., et al.: Remote controlled multishape polymer nanocomposites with selective radiofrequency actuations. *Adv. Mater.* **23**(28), 3192 (2011)
- Holzappel, G.A.: *Nonlinear Solid Mechanics: A Continuum Approach for Engineering*. Wiley, New York (2000)
- Huang, W.M., et al.: Water-driven programmable polyurethane shape memory polymer: demonstration and mechanism. *Appl. Phys. Lett.* **86**, 114105 (2005)
- Jiang, H.Y., Kelch, S., Lendlein, A.: Polymers move in response to light. *Adv. Mater.* **18**(11), 1471–1475 (2006)
- Jung, Y.C., So, H.H., Cho, J.W.: Water-responsive shape memory polyurethane block copolymer modified with polyhedral oligomeric silsesquioxane. *J. Macromol. Sci. B, Phys.* **45**(4), 453–461 (2006)
- Koerner, H., et al.: Remotely actuated polymer nanocomposites—stress-recovery of carbon-nanotube-filled thermoplastic elastomers. *Nat. Mater.* **3**(2), 115–120 (2004)
- Kovacs, A.J., et al.: Isobaric volume and enthalpy recovery of glasses. II. A transparent multiparameter theory. *J. Polym. Sci., Polym. Phys. Ed.* **17**(7), 1097–1162 (1979)
- Kumar, U.N., et al.: Non-contact actuation of triple-shape effect in multiphase polymer network nanocomposites in alternating magnetic field. *J. Mater. Chem.* **20**(17), 3404–3415 (2010)
- Lendlein, A., Kelch, S.: Shape-memory polymers. *Angew. Chem., Int. Ed. Engl.* **41**(12), 2035–2057 (2002)
- Lendlein, A., Kelch, S.: Shape-memory polymers as stimuli-sensitive implant materials. *Clin. Hemorheol. Microcirc.* **32**(2), 105–116 (2005)
- Lendlein, A., et al.: Light-induced shape-memory polymers. *Nature* **434**(7035), 879–882 (2005)
- Li, J.J., Xie, T.: Significant impact of thermo-mechanical conditions on polymer triple-shape memory effect. *Macromolecules* **44**(1), 175–180 (2011)
- Liu, Y.P., et al.: Thermomechanics of shape memory polymer nanocomposites. *Mech. Mater.* **36**(10), 929–940 (2004)
- Liu, Y.P., et al.: Thermomechanics of shape memory polymers: uniaxial experiments and constitutive modeling. *Int. J. Plast.* **22**(2), 279–313 (2006)
- Liu, C., Qin, H., Mather, P.T.: Review of progress in shape-memory polymers. *J. Mater. Chem.* **17**(16), 1543–1558 (2007)
- Long, K.N., et al.: Photomechanics of light-activated polymers. *J. Mech. Phys. Solids* **57**(7), 1103–1121 (2009)
- Long, K.N., et al.: Light-induced stress relief to improve flaw tolerance in network polymers. *J. Appl. Phys.* **107**, 053519 (2010a)
- Long, K.N., et al.: Photo-induced creep of network polymers. *Int. J. Struct. Ch. Solids* **2**, 41–52 (2010b)
- Long, K.N., Dunn, M.L., Qi, H.J.: Mechanics of soft active materials with phase evolution. *Int. J. Plast.* **26**(4), 603–616 (2010c)
- Long, K.N., Dunn, M.L., Qi, H.J.: Photo-induced deformation of active polymer films: single spot irradiation. *Int. J. Solids Struct.* **48**, 2089–2101 (2011)
- Mather, P.T., Luo, X.F., Rousseau, I.A.: Shape memory polymer research. *Annu. Rev. Mater. Res.* **39**, 445–471 (2009)

- McClung, A.J.W., Tandon, G.P., Baur, J.W.: Strain rate- and temperature-dependent tensile properties of an epoxy-based, thermosetting, shape memory polymer (Veriflex-E). *Mech. Time-Depend. Mater.* **16**(2), 205–221 (2012)
- McClung, A., Tandon, G., Baur, J.W.: Deformation rate-, hold time-, and cycle-dependent shape-memory performance of Veriflex-E resin. *Mech. Time-Depend. Mater.* **17**(1), 39–52 (2013)
- Mohr, R., et al.: Initiation of shape-memory effect by inductive heating of magnetic nanoparticles in thermoplastic polymers. *Proc. Natl. Acad. Sci. USA* **103**(10), 3540–3545 (2006)
- Morshedian, J., Khonakdar, H.A., Rasouli, S.: Modeling of shape memory induction and recovery in heat-shrinkable polymers. *Macromol. Theory Simul.* **14**(7), 428–434 (2005)
- Nguyen, T.D., et al.: A thermoviscoelastic model for amorphous shape memory polymers: incorporating structural and stress relaxation. *J. Mech. Phys. Solids* **56**(9), 2792–2814 (2008)
- Nguyen, T.D., et al.: Modeling the relaxation mechanisms of amorphous shape memory polymers. *Adv. Mater.* **22**(31), 3411–3423 (2010)
- Qi, H.J., Joyce, K., Boyce, M.C.: Durometer hardness and the stress–strain behavior of elastomeric materials. *Rubber Chem. Technol.* **76**(2), 419–435 (2003)
- Qi, H.J., et al.: Finite deformation thermo-mechanical behavior of thermally induced shape memory polymers. *J. Mech. Phys. Solids* **56**(5), 1730–1751 (2008)
- Rubinstein, M., Colby, R.H.: *Polymer Physics*. Oxford University Press, New York (2003)
- Ryu, J., et al.: Photo-origami. *Appl. Phys. Lett.* **100**, 161908 (2012)
- Schmidt, A.M.: Electromagnetic activation of shape memory polymer networks containing magnetic nanoparticles. *Macromol. Rapid Commun.* **27**(14), 1168–1172 (2006)
- Scott, T.F., et al.: Photoinduced plasticity in cross-linked polymers. *Science* **308**(5728), 1615–1617 (2005)
- Scott, T.F., Draughon, R.B., Bowman, C.N.: Actuation in crosslinked polymers via photoinduced stress relaxation. *Adv. Mater.* **18**(16), 2128 (2006)
- Sherrod, P.H.: Nonlinear regression analysis program, NLREG Version 5.0. (2000). Available from <http://www.nlreg.com/>
- Srivastava, V., Chester, S.A., Anand, L.: Thermally actuated shape-memory polymers: experiments, theory, and numerical simulations. *J. Mech. Phys. Solids* **58**(8), 1100–1124 (2010)
- Tobushi, H., et al.: Thermomechanical properties in a thin film of shape memory polymer of polyurethane series. *Smart Mater. Struct.* **5**(4), 483–491 (1996)
- Tobushi, H., Hashimoto, T., Ito, N.: Shape fixity and shape recovery in a film of shape memory polymer of polyurethane series. *J. Intell. Mater. Syst. Struct.* **9**, 127–136 (1998)
- Tool, A.Q.: Relation between inelastic deformability and thermal expansion of glass in its annealing range. *J. Am. Ceram. Soc.* **29**(9), 240–253 (1946)
- Tool, A.Q.: Effect of heat-treatment on the density and constitution of high-silica glasses of the borosilicate type. *J. Am. Ceram. Soc.* **31**(7), 177–186 (1948)
- Tool, A.Q., Eichlin, C.G.: Variations caused in the heating curves of glass by heat treatment. *J. Am. Ceram. Soc.* **14**(4), 276–308 (1931)
- Treloar, L.R.G.: *The Physics of Rubber Elasticity*. Monographs on the Physics and Chemistry of Materials, p. 342, 2nd edn. Clarendon Press, Oxford (1958)
- Wang, A., et al.: Programmable, pattern-memorizing polymer surface. *Adv. Mater.* **23**, 3669–3673 (2011)
- Weber, G., Anand, L.: Finite deformation constitutive-equations and a time integration procedure for isotropic, hyperelastic viscoplastic solids. *Comput. Methods Appl. Mech. Eng.* **79**(2), 173–202 (1990)
- Wei, Z.G., Sandstrom, R., Miyazaki, S.: Shape-memory materials and hybrid composites for smart systems—part I shape-memory materials. *J. Mater. Sci.* **33**(15), 3743–3762 (1998)
- Westbrook, K.K., et al.: Improved testing system for thermomechanical experiments on polymers using uniaxial compression equipment. *Polym. Test.* **29**(4), 503–512 (2010a)
- Westbrook, K.K., et al.: Constitutive modeling of shape memory effects in semicrystalline polymers with Stretch induced crystallization. *J. Eng. Mater. Technol.-Trans. ASME* **132**, 041010 (2010b)
- Westbrook, K.K., et al.: A 3D finite deformation constitutive model for amorphous shape memory polymers: a multi-branch modeling approach for nonequilibrium relaxation processes. *Mech. Mater.* **43**(12), 853–869 (2011)
- Westbrook, K.K., et al.: Two-way reversible shape memory effects in a free-standing polymer composite. *Smart Mater. Struct.* **20**, 065010 (2011)
- Williams, M.L., Landel, R.F., Ferry, J.D.: Temperature dependence of relaxation mechanisms in amorphous polymers and other glass-forming liquids. *Phys. Rev.* **98**(5), 1549 (1955)
- Xie, T.: Tunable polymer multi-shape memory effect. *Nature* **464**(7286), 267–270 (2010)
- Xie, T., Xiao, X.C., Cheng, Y.T.: Revealing triple-shape memory effect by polymer bilayers. *Macromol. Rapid Commun.* **30**(21), 1823–1827 (2009)
- Yakacki, C.M., et al.: Unconstrained recovery characterization of shape-memory polymer networks for cardiovascular applications. *Biomaterials* **28**(14), 2255–2263 (2007)

- Yu, K., et al.: Carbon nanotube chains in a shape memory polymer/carbon black composite: To significantly reduce the electrical resistivity. *Appl. Phys. Lett.* **98**, 074102 (2011)
- Yu, K., et al.: Mechanisms of multi-shape memory effects and associated energy release in shape memory polymers. *Soft Matter* **8**(20), 5687–5695 (2012)
- Yu, K., et al.: Design considerations for shape memory polymer composites with magnetic particles. *J. Compos. Mater.* **47**(1), 51–63 (2013)